Supporting Information

Mills et al. 10.1073/pnas.1321679111

SI Text

Alterations to COPSE Model

For this work, we use a simplified version of the carbon oxygen phosphorus sulphur evolution (COPSE) (1) biogeochemical model. All modifications are listed below. For the full model equations, see *Full Model Equations*; modifications 1–4 follow our previous work on the Neoproterozoic carbon cycle (2).

i) We assume phosphate is the limiting nutrient and remove the nitrate system from COPSE; this has been shown to make only minor changes to the Phanerozoic model predictions (3).

ii) The temperature dependence of the silicate weathering formulation is updated to be applicable to a broader temperature range. We follow the derivation of Berner (4) but do not make the simplifying assumption of temperature close to present day. The linear runoff approximation causes a singularity when temperature is low, and is amended by approximating the linear term with an exponential function. This gives an expression for the relative silicate weathering flux, assuming kinetic limitation.

$$f_T = e^{k_{s1}\frac{T-T_0}{TT_0}} \cdot \left(e^{k_{s2}(T-T_0)}\right)^{0.65}, \quad \text{[S1]}$$

where k_{s1} = 7537.69 and k_{s2} = 0.03. Here T is average surface temperature (K) and T_0 is present-day average surface temperature (288 K). Similarly, the linear runoff term for carbonate weathering is also approximated with an exponential:

$$g_T = e^{k_c(T-T_0)}, \quad \text{[S2]}$$

where k_c = 0.05. The temperature calculation follows COPSE (1), and planetary albedo is fixed at 0.3.

Transport limitation of terrestrial weathering (5) is not included in the final model. Extreme conditions are required for the global weathering flux to become transport limited (2), which are not encountered in any of the model runs presented in this work.

iii) COPSE defines the function *anox* which gives a numerical value $0 \le anox \le 1$ for the degree of ocean anoxia. The formulation used in the original model allows for negative values when ocean nutrient is very low. We truncate these to zero.

iv) Land organic carbon burial does not begin in COPSE until ∼450 Ma, which is beyond the timeframe we are interested in. It is removed from the model for this work.

v) Transfer of carbon from the hydrosphere to the crust via seafloor weathering is added to the model following the dynamic representation of Sleep and Zahnle (6):

$$sfw = k_{sfw}\left(\frac{dA}{dt}\right)(\mathrm{RCO_2})^{\alpha}, \quad \text{[S3]}$$

where $\frac{dA}{dt}$ is the relative spreading rate, RCO_2 denotes the relative concentration of CO_2 in the atmosphere, and $k_{sfw} = 1.75 \times 10^{12}$ mol/y is the assumed present-day rate, taken between current estimates (7–9). We follow ref. 6 in letting α expresses the dependency of hydrothermal carbonatization on ocean CO_2. The estimate of $\alpha = 0.23$ is obtained from a laboratory study (10) and used for the model baseline, being the only available data. Higher and lower estimates are also trialed.

vi) The fraction of atmosphere and ocean CO_2 that exists in the atmosphere is taken from an extension of COPSE (11) rather than assuming a constant fraction as in the published Phanerozoic model. We take $\mathrm{RCO_2} = e^{k_a(T_0-T)}\left(\frac{\Sigma CO_2}{(\Sigma CO_2)_0}\right)^2$, where ΣCO_2 is total carbon in the ocean, T is average surface temperature, and $k_a = -0.0448\ \mathrm{K}^{-1}$ is a constant.

vii) In COPSE, the present-day rate of silicate weathering (k_{silw}) is estimated via knowledge of other present-day fluxes and the assumption of steady state for CO_2. This gives a value of $k_{silw} = 6.65 \times 10^{12}$ mol/y. Addition of the seafloor weathering flux to this calculation reduces the value to $k_{silw} = 4.9 \times 10^{12}$ mol/y.

viii) The global spreading rate $\left(\frac{dA}{dt}\right)$ and uplift rate (U) over the Phanerozoic are imposed in COPSE as external forcings. We calculate the spreading rate forcing for 1.5–0.5 billion years ago (Ga) by scaling to the mantle heat flow (Q) estimates from refs. 6, 12, and 13, following the assumption that $\left(\frac{dA}{dt}\right) \approx Q^2$ (14). For this work, we take the uplift forcing to be constant at the present-day rate during the Precambrian, allowing changes in continental weathering efficiency via enhanced uplift to be represented instead by the parameter W. The remaining forcings in COPSE require no extension, as they either have value zero at the beginning of the Phanerozoic or, in the case of the solar forcing, are already well defined for the period of interest.

ix) Removal of ocean phosphate in COPSE occurs via burial with organics, and burial as either calcium-associated or iron-sorbed phosphorus (1, 15, 16). In the Pracambrian, it is expected that high silica concentration due to the lack of diatoms and radiolaria (17) would greatly inhibit phosphorus sorption onto ferric oxides (18). We therefore reduce the iron-sorbed phosphorus sink to zero for this work (see *Results and Discussion*). We also explore a scenario wherein calcium-associated phosphorus burial is also limited in the Precambrian due to high alkalinity (18); all model results from the article are reproduced for this scenario and shown in *Model Runs for Increased Nutrient Burial Limitation*.

x) In COPSE, degassing rates for buried pyrite and gypsum sulfur are not explicitly considered; they are instead represented by larger weathering fluxes. In this work, we are interested in the effects of a changing spreading rate, so we add the sulfur degassing fluxes to COPSE following their definition in the GEOCARBSULF (geochemical carbon and sulphur cycles) model (19). The partial calcium cycle trialed in COPSE is also removed for simplicity; this affects only the burial of gypsum.

xi) The present-day size of the crustal carbon reservoirs follows ref. 12, with the split between organic and carbonate carbon following the original COPSE model. This allows estimates of the size of these reservoirs in the Precambrian using model output from (12).

Full Model Equations

Full equations are documented below so that this work may be understood more easily without continual reference to the COPSE paper. Aside from the changes laid out in *Alterations to Copse Model*, they follow the original COPSE model (1). Equations that differ from COPSE are marked with an asterisk (*). RO_2 and RCO_2 denote concentrations of oxygen and carbon dioxide relative to present day. Subscript zeros represent the present-day size of fluxes and reservoirs.

List of Fluxes. Marine organic carbon burial*:

$$mocb = k_{mocb}\left(\frac{p}{p_0}\right)^2 \quad \text{[S4]}$$

Phosphorus weathering:

$$phosw = k_{phosw}\left(\frac{2}{12}\frac{silw}{silw_0}+\frac{5}{12}\frac{carbw}{carbw_0}+\frac{5}{12}\frac{oxidw}{oxidw_0}\right) \quad \text{[S5]}$$

Marine organic phosphorus burial:

$$mopb = \frac{mocb}{CPsea} \quad \text{[S6]}$$

Calcium-bound phosphorus burial:

$$capb = k_{capb}\frac{mocb}{mocb_0} \quad \text{[S7]}$$

Iron-sorbed phosphorus burial*:

$$fepb = 0 \quad \text{[S8]}$$

Silicate weathering:

$$silw = k_{silw}\cdot W\cdot U\cdot f_T\cdot\sqrt{\mathrm{RCO_2}} \quad \text{[S9]}$$

Carbonate weathering:

$$carbw = k_{carbw}\cdot W\cdot U\cdot g_T\cdot\sqrt{\mathrm{RCO_2}} \quad \text{[S10]}$$

Oxidative weathering:

$$oxidw = k_{oxidw}\cdot U\cdot\sqrt{\mathrm{RO_2}} \quad \text{[S11]}$$

Marine carbonate carbon burial:

$$mccb = silw + carbw \quad \text{[S12]}$$

Seafloor weathering*:

$$sfw = k_{sfw}\left(\frac{dA}{dt}\right)(\mathrm{RCO_2})^{\alpha} \quad \text{[S13]}$$

Pyrite sulfur weathering:

$$pyrw = k_{pyrw}\cdot U\cdot\frac{PYR}{PYR_0}\sqrt{\mathrm{RO_2}} \quad \text{[S14]}$$

Gypsum sulfur weathering:

$$gypw = k_{gypw}\cdot U\cdot\frac{GYP}{GYP_0}\cdot\frac{carbw}{carbw_0} \quad \text{[S15]}$$

Pyrite sulfur burial:

$$mpsb = k_{mpsb}\cdot\frac{s}{s_0}\cdot\frac{1}{o}\cdot\frac{mocb}{mocb_0} \quad \text{[S16]}$$

Gypsum sulfur burial*:

$$mgsb = k_{mgsb}\cdot\frac{s}{s_0} \quad \text{[S17]}$$

Pyrite sulfur degassing:

$$pyrdeg = k_{pyrdeg}\left(\frac{PYR}{PYR_0}\right)\frac{dA}{dt} \quad \text{[S18]}$$

Gypsum sulfur degassing:

$$gypdeg = k_{gypdeg}\left(\frac{GYP}{GYP_0}\right)\frac{dA}{dt} \quad \text{[S19]}$$

Organic carbon degassing:

$$ocdeg = k_{ocdeg}\left(\frac{G}{G_0}\right)\frac{dA}{dt} \quad \text{[S20]}$$

Carbonate carbon degassing:

$$ccdeg = k_{ccdeg}\left(\frac{C}{C_0}\right)\frac{dA}{dt}. \quad \text{[S21]}$$

Other Calculations. Relative atmospheric CO_2*:

$$\mathrm{RCO_2} = e^{k_a(T_0-T)}\left(\frac{\Sigma\mathrm{CO_2}}{(\Sigma\mathrm{CO_2})_0}\right)^2, \quad \text{[S22]}$$

where ΣCO_2 is total oceanic carbon

Relative atmospheric O_2:

$$\mathrm{RO_2} = \frac{\frac{O}{O_0}}{\frac{O}{O_0}+k_{\mathrm{O2}}}, \quad \text{[S23]}$$

where $k_{O2} = 3.762$

Solar forcing:

$$S = \frac{S_0}{1+0.38\left(\frac{t}{\tau}\right)}, \quad \text{[S24]}$$

where $S_0 = 1368\ \mathrm{W\cdot m^{-2}}$ and $\tau = 4.55\times10^9$ years.

Following COPSE, the global average surface temperature calculation is taken from the model of Caldeira and Kasting (20) and requires inputs of solar forcing, albedo, and carbon dioxide concentration. This follows the COPSE treatment.

Reservoir Calculations. Ocean phosphate:

$$\frac{dP}{dt} = phosw - mopb - capb - fepb \quad \text{[S25]}$$

Hydrosphere carbon*:

$$\frac{dA}{dt} = carbw + ccdeg + oxidw + ocdeg - mccb - mocb - sfw \quad \text{[S26]}$$

Ocean sulfate:

$$\frac{ds}{dt} = pyrw + pyrdeg + gypw + gypdeg - mpsb - mgsb \quad \text{[S27]}$$

Buried organic C:

$$\frac{dG}{dt} = mocb - oxidw - ocdeg \quad \text{[S28]}$$

Buried carbonate C *:

$$\frac{dC}{dt} = mccb + sfw - carbw - ccdeg \quad \textbf{[S29]}$$

Buried pyrite S:

$$\frac{dPYR}{dt} = mpsb - pyrw - pyrdeg \quad \textbf{[S30]}$$

Buried Gypsum S:

$$\frac{dPYR}{dt} = mgsb - gypw - gypdeg. \quad \textbf{[S31]}$$

Present-day values	Source
Marine organic carbon burial: $k_{mocb} = 4.5 \times 10^{12}$ mol C yr^{-1}	COPSE
Calcium-bound P burial: $k_{capb} = 1.5 \times 10^{10}$ mol P yr^{-1}	COPSE
Pyrite sulfur burial*: $k_{mpsb} = 7 \times 10^{11}$ mol S yr^{-1}	for steady state
Gypsum sulfur burial*: $k_{mgsb} = 2.5 \times 10^{12}$ mol S yr^{-1}	for steady state
Silicate weathering*: $k_{silw} = 4.9 \times 10^{12}$ mol C y^{-1}	for steady state
Seafloor weathering*: $k_{sfw} = 1.75 \times 10^{12}$ mol C y^{-1}	refs. 7–9
Oxidative weathering: $k_{oxidw} = 7.75 \times 10^{12}$ mol C y^{-1}	for steady state
Reactive P weathering: $k_{phosw} = 4.9 \times 10^{10}$ mol P y^{-1}	for steady state
Pyrite sulfur weathering: $k_{pyrw} = 4.5 \times 10^{11}$ mol S y^{-1}	GEOCARBSULF
Gypsum sulfur weathering: $k_{gypw} = 2 \times 10^{12}$ mol S y^{-1}	GEOCARBSULF
Organic carbon degassing: $k_{ocdeg} = 1.25 \times 10^{12}$ mol C y^{-1}	COPSE
Carbonate carbon degassing: $k_{ccdeg} = 6.65 \times 10^{12}$ mol C y^{-1}	COPSE
Pyrite sulfur degassing: $k_{pyrdeg} = 2.5 \times 10^{11}$mol S y^{-1}	GEOCARBSULF
Gypsum sulfur degassing: $k_{gypdeg} = 5. \times 10^{11}$ mol S y^{-1}	GEOCARBSULF
Atmosphere and ocean CO_2: $A_0 = 3.193 \times 10^{18}$ mol	COPSE
Ocean phosphate: $P_0 = 3.1 \times 10^{15}$ mol	COPSE
Ocean sulfate: $P_0 = 4 \times 10^{19}$ mol	COPSE
Atmosphere and ocean oxygen: $O_0 = 3.7 \times 10^{19}$ mol	COPSE
Buried organic carbon*: $G_0 = 1.9 \times 10^{21}$ mol	COPSE and ref. 12
Buried carbonate carbon*: $C_0 = 6.6 \times 10^{21}$ mol	COPSE and ref. 12
Buried pyrite sulfur: $PYR_0 = 1.8 \times 10^{20}$ mol	COPSE
Buried gypsum sulfur: $GYP_0 = 2 \times 10^{20}$ mol	COPSE
Carbon-to-phosphorus burial ratio (*CPsea*): 250 mol/mol	COPSE

Forcings	Attributes
Relative seafloor spreading rate	$\frac{dA}{dt} = 1$ for present day, scaling relationship from (6, 13)
Relative uplift rate	$U = 1$ for present day. Fixed at present-day value for Precambrian, COPSE forcing for Phanerozoic
Terrestrial weatherability	W = 1 for present day, W $\approx \frac{1}{4}$ before vascular plants (19)

Terrestrial Weatherability and Oxidative Weathering

In previous carbon cycle models, changes in terrestrial weatherability are assumed to impact the fluxes of silicate and carbonate weathering only (21). However, it may be possible that processes that increase mechanical weathering rates also influence the oxidative weathering of organic matter. Under this assumption, increasing terrestrial weatherability would lead to increased oxygen consumption by oxidative weathering, potentially countering the oxygen rise from increased nutrient delivery. Fig. S1 shows steady states of the COPSE model with respect to terrestrial weatherability, W, for a scenario in which W impacts the oxidative weathering flux (as a multiplier in the same way it is added to silicate and carbonate weathering). It can be seen that the dynamics of the system are not substantially altered—because as well as consuming oxygen, oxidative weathering is assumed to deliver phosphorous to the ocean, which boosts productivity. The overall effect is a slight weakening of the relationship between W and steady state oxygen concentration. For $\alpha > 0.15$, the qualitative dynamics are unchanged.

Effects of Altering Global Spreading Rate at 500 Ma

In the main text, steady states are plotted at 1,000 Ma, at the midpoint of the timeframe of interest. It is shown that an increase in spreading rate leads to both higher CO_2 degassing (resulting in more C burial) and a shift in the dominant C removal pathway toward seafloor weathering (resulting in less nutrient input per weathered amount of C). At 500 Ma, it is assumed that the crustal content of carbon is higher than at 1,000 Ma (following ref. 12). This amplifies any change in the degassing rate and therefore weakens the effect of changing spreading rate on O_2 concentration. At steady state, oxygen decreases under an increase in spreading rate for $\alpha \geq 0.23$.

Model Runs for Increased Nutrient Burial Limitation

The following figures are run for the same conditions as the model output shown in the main article, with one alteration: The flux of calcium associated phosphorus burial is limited by reducing k_{capb} to 50% of its value in COPSE. Here $k_{capb} = 7.5 \times 10^9$ mol P y^{-1}. This is an arbitrary reduction used to explore the possibility of extremely harsh limitations on the burial of phosphate in the Precambrian due to high alkalinity (18). A dynamical representation of limitation of phosphorus burial due to changing silica concentration and alkalinity would be better suited; however, this is beyond the scope of this work. The model runs here were performed to assess whether higher P burial limitation might alter the dynamics of the carbon removal balance. Results do not show a qualitative difference from those in the main text; however, it is demonstrated that a more powerful relationship between seafloor weathering and atmospheric CO_2 concentration is required for O_2 to decrease under an increase in

spreading rate when nutrient burial is more strongly limited (see main text).

Figures S3–S6 are comparable to Figs. 2–5, respectively.

Model Runs for Alternative Heat Flow Parameterization

Fig. S7 shows steady states at discrete time points when forced with the mantle heat flow estimate of Korenaga (31). Korenaga's model predicts a slowly increasing heat flow, and therefore spreading rate, over the Proterozoic. The increase in heat flow acts to decrease oxygen concentration, which contrasts with the increase in solar constant, which acts to increase steady state oxygen. The result is a very slow oxygen rise over the model timeframe, rather than the sharper rise predicted by the baseline model.

Computing Steady State Solutions

The modified COPSE model is run to steady state for changes in the terrestrial weathering enhancement parameter W, spreading rate, solar forcing, or the time point, t. All model forcings are held constant at the value for the given time point, and the total crustal inventory of carbon for time t is set using model output from Hayes and Waldbauer (12). Model runs were performed using the MATLAB ODE suite variable time step solvers (32); steady state is verified for each run over a 100-Gy timeframe. The COPSE model becomes unstable for $RO_2 << 10^{-3}$ due to lack of representation of the anoxic biosphere. This limits the range of parameter choices for high values of α. However, all expected variation over 1,500–500 Ma is within the model capability.

1. Bergman NM, Lenton TM, Watson AJ (2004) COPSE: A new model of biogeochemical cycling over Phanerozoic time. *Am J Sci* 304(5):397–437.
2. Mills B, Watson AJ, Goldblatt C, Boyle R, Lenton TM (2011) Timing of Neoproterozoic glaciations linked to transport-limited global weathering. *Nat Geosci* 4:861–864.
3. Mills B (2012) Weathering pathways and limitations in biogeochemical models: Application to Earth system evolution. PhD thesis (Univ of East Anglia, Norwich, UK).
4. Berner RA (1994) GEOCARB II: A revised model of atmospheric CO_2 over Phanerozoic time. *Am J Sci* 294(1):56–91.
5. West AJ, Galy A, Bickle M (2005) Tectonic and climatic controls on silicate weathering. *Earth Planet Sci Lett* 235(1-2):211–228.
6. Sleep NH, Zahnle K (2001) Carbon dioxide cycling and implications for climate on ancient Earth. *J Geophys Res* 106(E1):1373–1399.
7. Gillis KM, Coogan LA (2011) Secular variation in carbon uptake into the ocean crust. *Earth Planet Sci Lett* 302(3-4):385–392.
8. Alt JC, Teagle DAH (1999) The uptake of carbon during alteration of oceanic crust. *Geochim Cosmochim Acta* 63:1527–1535.
9. Staudigel H, Hart SR, Schmincke H-U, Smith BM (1989) Cretaceous ocean crust at DSDP sites 417 and 418: Carbon uptake from weathering verses loss by magmatic outgassing. *Geochim Cosmochim Acta* 53:3091–3094.
10. Brady PV, Gislason SR (1997) Seafloor weathering controls on atmospheric CO_2 and global cimate. *Geochim Cosmochim Acta* 61:965–973.
11. Bergman NM (2003) COPSE: A new biogeochemical Earth system model for the Phanerozoic. PhD thesis(Univ of East Anglia, Norwich. UK).
12. Hayes JM, Waldbauer JR (2006) The carbon cycle and associated redox processes through time. *Philos Trans R Soc Lond B Biol Sci* 361(1470):931–950.
13. Lowell RP, Keller SM (2003) High-temperature seafloor hydrothermal circulation over geologic time and Archean banded iron formations. *Geophys Res Lett* 30(7):1391.
14. Franck S, Bounama C (1997) Continental growth and volatile exchange during Earth's evolution. *Phys Earth Planet Inter* 100(1-4):189–196.
15. VanCappellen P, Ingall ED (1994) Benthic phosphorus regeneration, net primary production, and ocean anoxia: A model of the coupled marine biogeochemical cycles of carbon and phosphorus. *Paleoceanography* 9(5):677–692.
16. Van Cappellen P, Ingall ED (1996) Redox stabilization of the atmosphere and oceans by phosphorus-limited marine productivity. *Science* 271(5248):493–496.
17. Racki G, Cordey F (2000) Radiolarian palaeoecology and radiolarites: Is the present the key to the past? *Earth Sci Rev* 52(1-3):83–120.
18. Planavsky NJ, et al. (2010) The evolution of the marine phosphate reservoir. *Nature* 467(7319):1088–1090.
19. Berner RA (2006) GEOCARBSULF: A combined model for Phanerozoic atmospheric O_2 and CO_2. *Geochim Cosmochim Acta* 70:5653–5664.
20. Caldeira K, Kasting JF (1992) The life span of the biosphere revisited. *Nature* 360(6406):721–723.
21. Berner RA (1991) A model for atmospheric CO_2 over Phanerozoic time. *Am J Sci* 291(4): 339–376.
22. Gaffin S (1987) Ridge volume dependence on seafloor generation rate and inversion using long term sealevel change. *Am J Sci* 287(6):596–611.
23. Kump LR (2008) The rise of atmospheric oxygen. *Nature* 451(7176):277–278.
24. Canfield DE, Poulton SW, Narbonne GM (2007) Late-Neoproterozoic deep-ocean oxygenation and the rise of animal life. *Science* 315(5808):92–95.
25. Kah LC, Lyons TW, Frank TD (2004) Low marine sulphate and protracted oxygenation of the Proterozoic biosphere. *Nature* 431(7010):834–838.
26. Sheldon ND (2013) Causes and consequences of low atmospheric pCO_2 in the Late Mesoproterozoic. *Chem Geol* 362:224–231.
27. Kah LC, Riding R (2007) Mesoproterozoic carbon dioxide levels inferred from calcified cyanobacteria. *Geology* 35(9):799–802.
28. Kaufman AJ, Xiao S (2003) High CO_2 levels in the Proterozoic atmosphere estimated from analyses of individual microfossils. *Nature* 425(6955):279–282.
29. Kah LC, Bartley JK (2004) Effect of marine carbon reservoir size on the duration of carbon isotope excursions: Interpreting the Mesoproterozoic carbon isotope record. *Geol Soc Am Abstr Programs* 36(5):78.
30. Hoffman PF, Schrag DP (2002) The snowball Earth hypothesis: Testing the limits of global change. *Terra Nova* 14(3):129–155.
31. Korenaga J (2008) Plate tectonics, flood basalts and the evolution of Earth's oceans. *Terra Nova* 20(6):419–439.
32. Shampine LF, Reichelt MW (1997) The Matlab ODE suite. *SIAM J Sci Comput* 18(1):1–22.

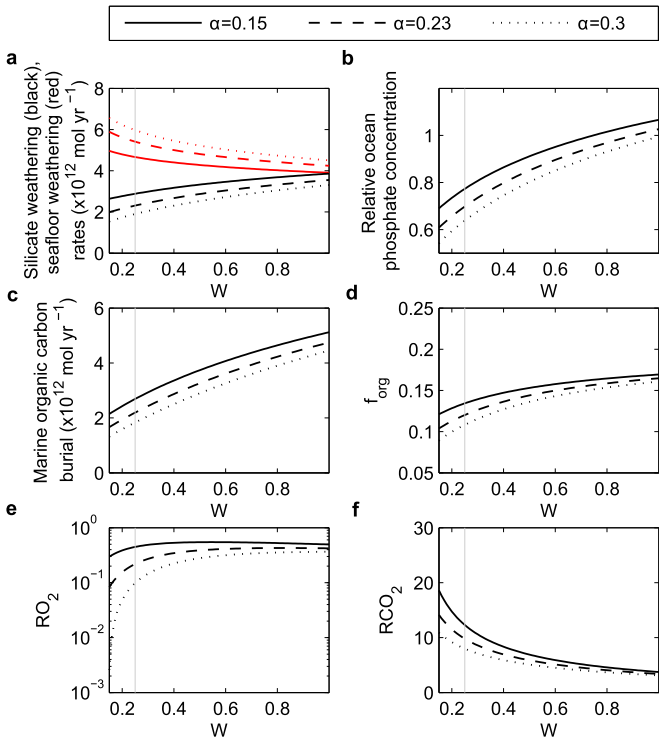

Fig. S1. Model steady states at 1,000 Ma against terrestrial weatherability, W (W affects oxidative weathering flux). Line type shows choices for the dependency of seafloor weathering rate on atmospheric CO_2 concentration. Rates of silicate and seafloor weathering (*A*), relative ocean phosphate concentration (*B*), organic carbon burial rate (*C*), the fraction of carbon buried organically (*D*), relative atmospheric oxygen (*E*), and CO_2 concentrations (*F*). Gray vertical line denotes best guess for W at 1,000 Ma (19).

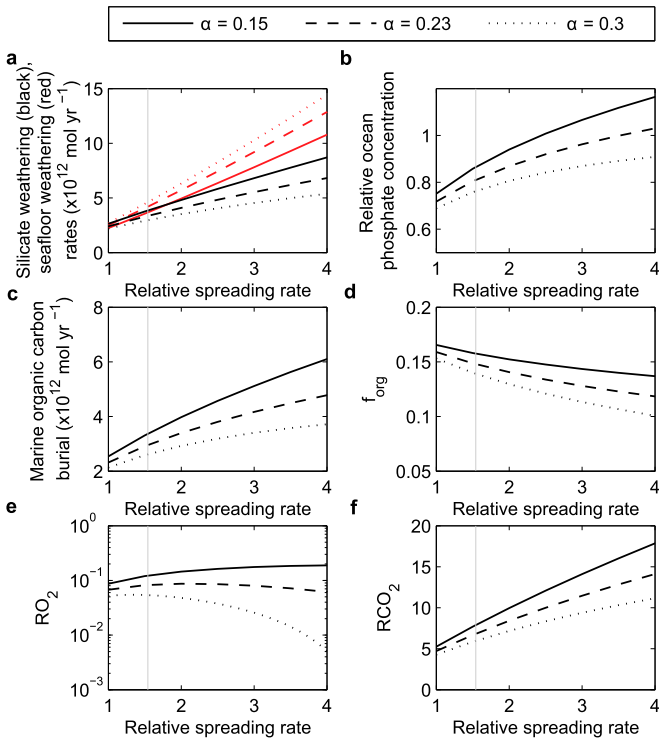

Fig. S2. Model steady states at 500 Ma against relative seafloor spreading rate. Line type shows choices for the dependency of seafloor weathering rate on atmospheric CO_2 concentration. Rates of silicate and seafloor weathering (*A*), relative ocean phosphate concentration (*B*), organic carbon burial rate (*C*), the fraction of carbon buried organically (*D*), relative atmospheric oxygen (*E*), and CO_2 concentrations (*F*). Gray vertical line denotes assumed spreading rate at 500 Ma (22).

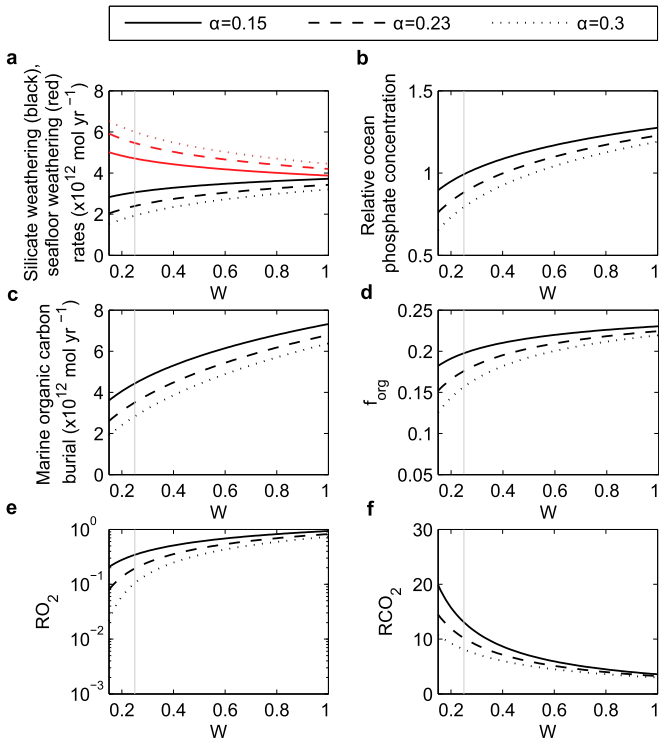

Fig. S3. Model steady states at 1,000 Ma against terrestrial weatherability, W. Line type shows choices for the dependency of seafloor weathering rate on atmospheric CO_2 concentration. Rates of silicate and seafloor weathering (*A*), relative ocean phosphate concentration (*B*), organic carbon burial rate (*C*), the fraction of carbon buried organically (*D*), relative atmospheric oxygen (*E*), and CO_2 concentrations (*F*). Gray vertical line denotes best guess for W at 1,000 Ma (19). K_{capb} is reduced by 50% for this run.

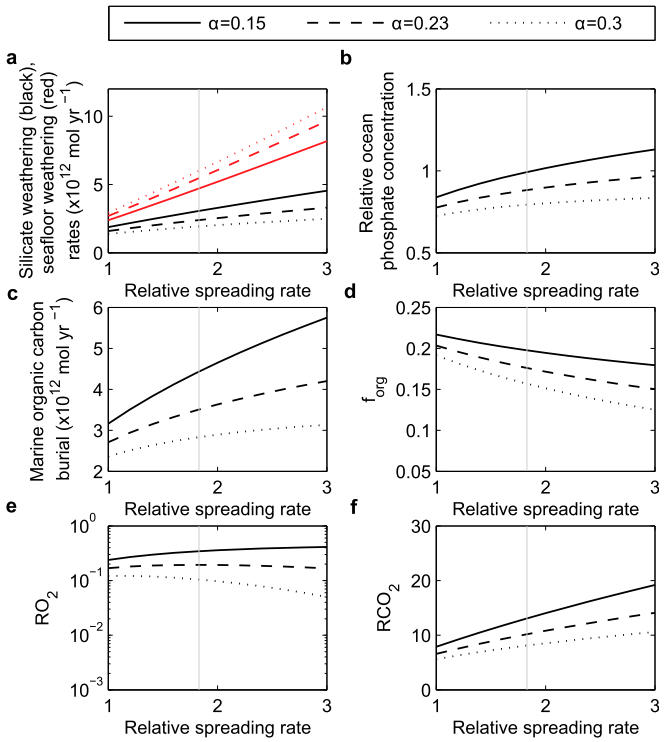

Fig. S4. Model steady states at 1,000 Ma against relative seafloor spreading rate. Line type shows choices for the dependency of seafloor weathering rate on atmospheric CO_2 concentration. Rates of silicate and seafloor weathering (*A*), relative ocean phosphate concentration (*B*), organic carbon burial rate (*C*), the fraction of carbon buried organically (*D*), relative atmospheric oxygen (*E*), and CO_2 concentrations (*F*). Gray vertical line denotes assumed spreading rate at 1,000 Ma (13). K_{capb} is reduced by 50% for this run.

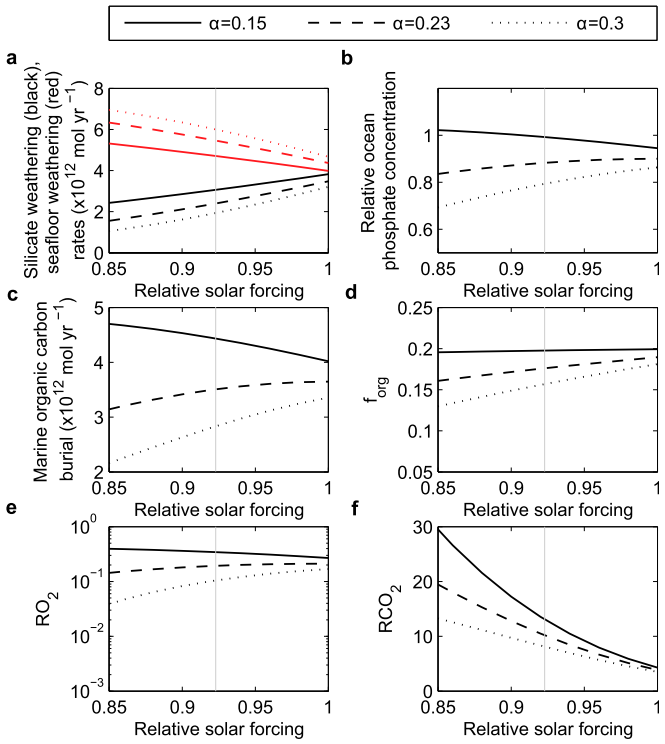

Fig. S5. Model steady states at 1,000 Ma against relative solar flux. Line type shows choices for the dependency of seafloor weathering rate on atmospheric CO_2 concentration. Rates of silicate and seafloor weathering (*A*), relative ocean phosphate concentration (*B*), organic carbon burial rate (*C*), the fraction of carbon buried organically (*D*), relative atmospheric oxygen (*E*), and CO_2 concentrations (*F*). Gray vertical line denotes assumed solar flux at 1,000 Ma (20). K_{capb} is reduced by 50% for this run.

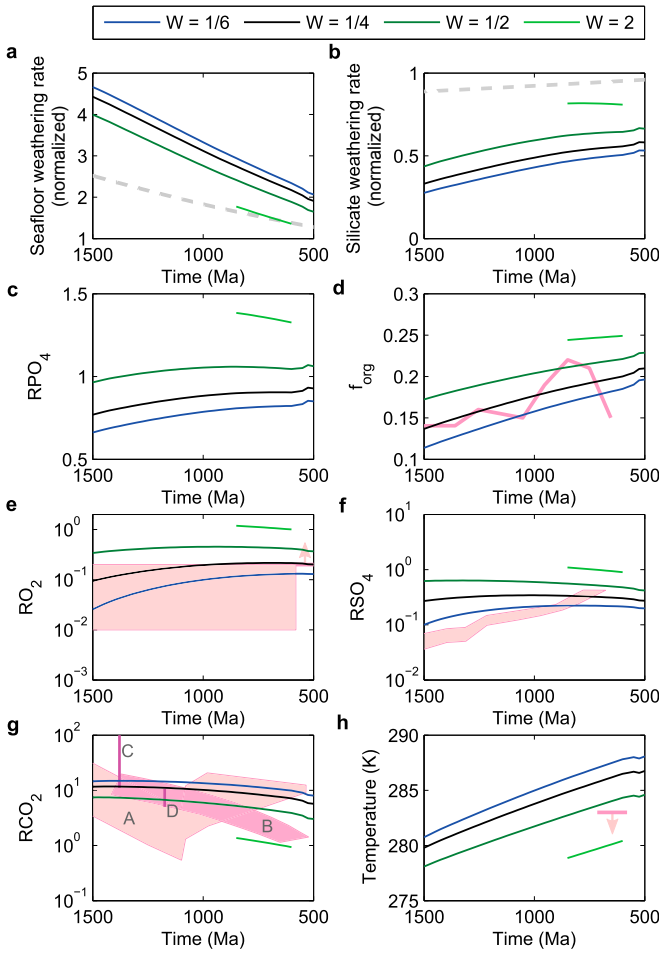

Fig. S6. Model steady states at discrete time points for 1,500–500 Ma for $\alpha = 0.23$. Line color denotes relative weatherability of the continents, W. Relative spreading rate (13) shown as gray dashed line in *A*; relative solar forcing (20) shown as gray dashed line in *B*. Geological constraints are shown in pink. Plotted are normalized rates of seafloor (*A*) and silicate (*B*) weathering, relative ocean phosphate concentration (*C*), the fraction of carbon buried organically (*D*), relative atmospheric oxygen concentration against the constraints from refs. 23 and 24 (*E*), relative ocean sulfate concentration against ref. 25 (*F*), relative CO_2 concentration against data from refs. 26–29 (*G*), and global average surface temperature shown with expected low temperature during the Neoproterozoic glacial period (30) (*H*). K_{capb} is reduced by 50% for this run.

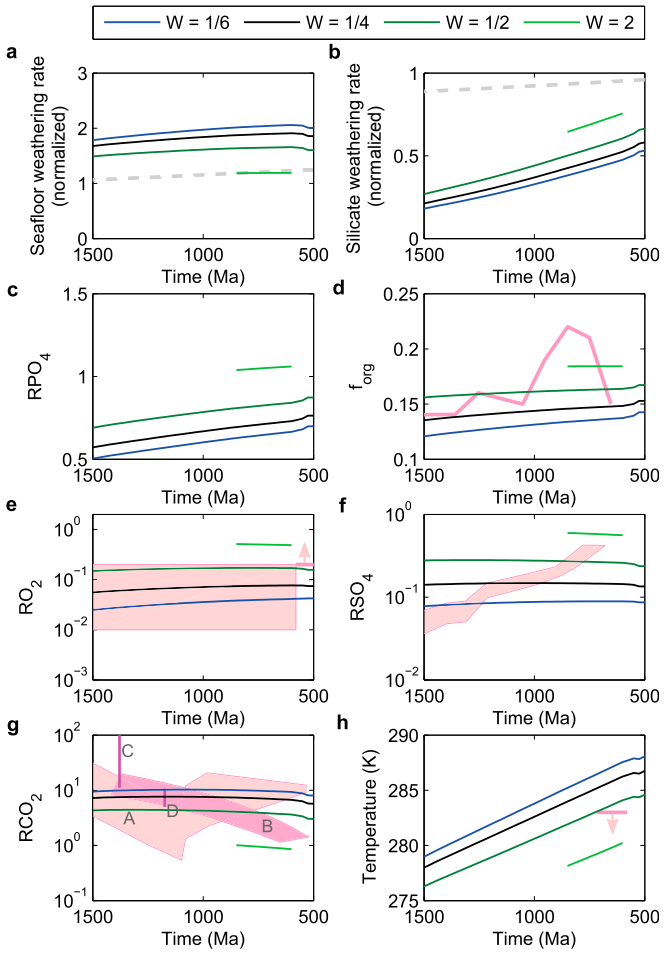

Fig. S7. Model steady states at discrete time points for 1,500–500 Ma for $\alpha = 0.23$ and increasing mantle heat flow. Line color denotes relative weatherability of the continents, W. Relative spreading rate (31) shown as gray dashed line in *A*; relative solar forcing (20) shown as gray dashed line in *B*. Geological constraints are shown in pink. Plotted are normalized rates of seafloor (*A*) and silicate (*B*) weathering, relative ocean phosphate concentration (*C*), the fraction of carbon buried organically (*D*), relative atmospheric oxygen concentration against the constraints from refs. 23 and 24 (*E*), relative ocean sulfate concentration against ref. 25 (*F*), relative CO_2 concentration against data from refs. 26–29 (*G*), and global average surface temperature shown with expected low temperature during the Neoproterozoic glacial period (30) (*H*).